HHS Public Access

Author manuscript

Cell Metab. Author manuscript; available in PMC 2019 January 09.

Published in final edited form as:

Cell Metab. 2018 January 09; 27(1): 252–262.e3. doi:10.1016/j.cmet.2017.12.004.

An Adipose Tissue Atlas: An Image Guided Identification of Human-like BAT and Beige Depots in Rodents

Fang Zhang[1,2], **Guiyang Hao**[3], **Mengle Shao**[2], **Gedaa Hassan**[3], **Yu An**[2], **Qiong Wang**[2], **Yi Zhu**[2], **Christine M. Kusminski**[2], **Kien Nham**[3], **Rana K. Gupta**[2], **Qiwei Zhai**[1], **Xiankai Sun**[3], **Philipp E. Scherer**[2,4,*], and **Orhan K. Oz**[3,*]

[1]Key Laboratory of Nutrition and Metabolism, Institute for Nutritional Sciences, Shanghai Institutes for Biological Sciences, Chinese Academy of Sciences, Shanghai 200031, China

[2]Touchstone Diabetes Center, Department of Internal Medicine, University of Texas Southwestern Medical Center, Dallas, TX 75390, USA

[3]Department of Radiology, University of Texas Southwestern Medical Center, Dallas, TX 75390-8542, USA

SUMMARY

[^{18}F]-Fluorodeoxyglucose-PET/CT (^{18}F-FDG-PET/CT) imaging has been invaluable for visualizing metabolically active adipose tissues in humans with potential anti-diabetic and anti-obesity effects. To explore whether mice display human-like fat depots in anatomically comparable regions, we mapped fat depots using glucose or fatty acid imaging tracers, such as ^{18}F-FDG through PET/CT or [$^{123/125}$I]-β-Methyl-*p*-iodophenyl-pentadecanoic acid ($^{123/125}$I-BMIPP) with SPECT/CT imaging, to analogous depots in mice. Using this type of image analysis with both probes, we define a large number of additional areas of high metabolic activity corresponding to novel fat pads. Histological and gene expression analysis validate these regions as *bona fide* fat pads. Our findings indicate that rodents show a high degree of topological similarity of fat depots to humans. Studies involving both glucose and lipid tracers indicate differential preferences for these substrates in different depots and also suggest that fatty acid based visualized approaches may reveal additional BAT and beige depots in humans.

[*]Correspondence: Philipp.scherer@utsouthwestern.edu, Orhan.Oz@utsouthwestern.edu.
[4]Lead Contact

AUTHOR CONTRIBUTIONS

F.Z. conceived, designed, performed most of the experiments and analyzed the data. G.H. and K.N. performed the PET/CT and SPECT/CT scanning experiments. G.H. performed the radiochemistry and participated in the image analysis. G.H. and K.N. analyzed the scanning images. M.S. provided FAT-ATTAC mice. Y.A. conducted part of the immunostaining. P.E.S. and O.K.O. conceived, designed, and supervised the project. F.Z., P.E.S and O.K.O. wrote the manuscript. Q.W., Y.Z., C.M.K., R.K.G, Q.Z. and X.S. provided expertise and feedback on the manuscript.

Conflicts of interest: none.

SUPPLEMENTAL INFORMATION

Supplemental Information includes one Table, nine 3D-movies and four Figures.

eTOC Blurb

^{18}F-FDG-PET/CT imaging in humans has been invaluable for visualizing metabolically active adipose tissues. Using PET/CT and SPECT/CT for imaging glucose and lipid metabolism in mice respectively, Zhang et al. define an atlas of fat depots, topologically analogous to those observed in humans.

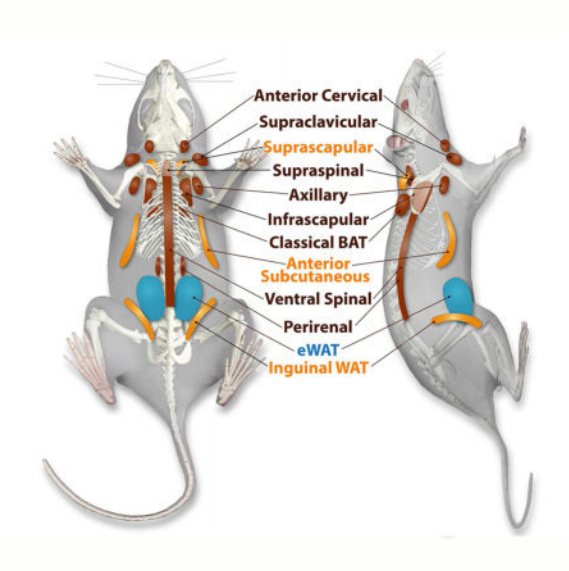

INTRODUCTION

The global epidemic of obesity and type 2 diabetes has greatly increased interest in the distribution and function of different adipose tissues. Three different types of adipocytes have been described, including white, beige and brown fat cells (Scherer, 2016). White fat cells are specialized in the storage of energy in the form of triglycerides and secrete important hormone-like molecules such as leptin and adiponectin to influence processes such as food intake, insulin sensitivity, and insulin secretion (Scherer, 2006). Thermogenic fat cells include brown and beige adipocytes, cells that play a critical role in defending against hypothermia, obesity and diabetes through dissipating chemical energy as heat via mitochondrial uncoupling protein 1 (UCP1) - mediated pathways and potentially through the release of a distinct set of secreted molecules (Betz and Enerback, 2015). Brown adipocytes express constitutively higher levels of thermogenic genes, whereas beige adipocytes are thought to develop in white adipose tissue in response to various activators, such as cold exposure and β3 adrenergic stimulation (Cannon and Nedergaard, 2004; Harms and Seale, 2013; Wu et al., 2012). It has been estimated in humans that 50g of white adipose tissues can store about 300 kcal energy, while as little as 50g of brown adipose tissue (BAT) can utilize up to 300 kcal energy daily if maximally stimulated (Rothwell and Stock, 1983). Therefore, these fat depots with some degree of thermogenic activity are therefore recognized as targets with therapeutic potential (Cohen and Spiegelman, 2016).

The long-standing prevailing view was that rodents and other small mammals have copious brown fat depots, but larger mammals often lose their prominent brown fat depots after infancy (Sidossis and Kajimura, 2015). However, [^{18}F]-Fluorodeoxyglucose-Positron Emission Tomography–Computed Tomography (^{18}F-FDG-PET/CT) scans demonstrated active BAT exists in the supraclavicular and neck areas of adult humans (Hany et al., 2002). Subsequently, other studies utilizing ^{18}F-FDG-PET/CT indicated active BAT depots present in adult humans that could be readily activated with cold exposure (Cypess et al., 2009; Mirbolooki et al., 2011; Nedergaard et al., 2007; Orava et al., 2011; Saito et al., 2009; van Marken Lichtenbelt et al., 2009; Virtanen et al., 2009). Therefore, ^{18}F-FDG-PET/CT has become the *de facto* imaging method to reveal the presence and function of activated BAT in humans.

The presence of BAT in humans and its potential therapeutic function is however challenging to study. Moreover, it is not clear that FDG uptake is the best or sole imaging biomarker for identifying metabolically active fat. For further metabolic and molecular characterization, it would be helpful to identify adipose tissues in rodents that are analogous to the ones identified in humans. Systemic studies on thermogenic adipose tissues in the mouse could in turn explore the presence of functional fat depots with metabolic activities similar to humans. Considering glucose and fatty acids are two main energy substrates for fat tissues (Jensen, 2002; Rosen and Spiegelman, 2006; Townsend and Tseng, 2014), we set out to map metabolically active fat tissues through visualizing uptake of radioactive derivatives of these substrates into adipose tissues. ^{18}F-FDG-PET/CT provides an image-guided approach to visualize fat pads with the ability to perform glucose uptake in mouse models (Hao et al., 2013; Mirbolooki et al., 2014; Wang et al., 2012). We also aimed to complement the map generated for tissues with avid glucose uptake by comparing them to tissues with high fatty acid uptake. [$^{123/125}$I]-β-Methyl-*p*-iodophenyl-pentadecanoic acid ($^{123/125}$I-BMIPP), as labeled with the single-photon emitting isotopes Iodine-123 or Iodine-125, is a branched long-chain fatty acid radiopharmaceutical with trapping in triglyceride pools and slow oxidation, and is a widely-used tracer in clinical cardiac imaging studies (Goodman et al., 1984; Knapp and Kropp, 1999; Peterson and Gropler, 2010; Taki and Matsunari, 2007). It is well-suited for Single-Photon Emission Computed Tomography–Computed Tomography (SPECT/CT) imaging to evaluate the signal distribution based on the uptake of fatty acids into fat tissues. Hence, we utilized $^{123/125}$I-BMIPP-SPECT/CT as a complementary approach to enhance our chances to identify additional depots that were less obviously visualized by ^{18}F-FDG-PET/CT scanning.

Our strategy was to comprehensively map metabolically active fat pads using the three-dimensional (3D) distribution of ^{18}F-FDG glucose and ^{123}I-BMIPP fatty acid uptake as guides. An inducible fat ablation mouse model, histological analysis and marker gene identification were subsequently used to identify the discrete nature of these regions and classify them into white, brown or beige fat depots based on their gene expression analysis.

RESULTS

Human Thermogenic Tissues Activity as Assessed by ^{18}F-FDG-PET/CT for Glucose Uptake

The ^{18}F-FDG-PET/CT-scanning method has defined regions of functionally active UCP1-positive brown adipose tissue in adult humans (Cypess et al., 2009; Enerback, 2010; Mirbolooki et al., 2011; van Marken Lichtenbelt et al., 2009). It also provides us with an opportunity to identify systemic human-like thermogenic fat tissues in rodents. To map the human-like metabolically active adipose in mice, we first generated 3D-images of human active thermogenic adipose after ^{18}F-FDG glucose uptake. As shown in Figure 1, cervical, supraclavicular and axillary areas were the regions with prominent activity of glucose uptake at room temperature among all adipose tissues. Paravertebral and peri-renal tissues also showed activity. To better visualize the accurate localization of these depots of high glucose uptake activity, a 3D-movie is also provided (Movie S1). For the subject in the supplemental movie, his most active thermogenic tissues labeled by the glucose analogue were at the back of the neck and in the supraclavicular region, with reduced activity in the anterior cervical region.

Regions of High Metabolic Activity in Mice as Assessed by 3D-images of PET/CT with ^{18}F-FDG for Glucose Uptake and SPECT/CT with ^{123}I-BMIPP for Fatty Acid Uptake

To investigate fat depots with high metabolic activity in rodents, we utilized the same ^{18}F-FDG-PET/CT-scanning approach as in humans to present the 3D-images of glucose uptake and distribution in functionally active adipose tissues of mice. C57BL/6 mice housed at room temperature showed the strongest signals around classical interscapular BAT (iBAT) as well as infrascapular regions. Supraclavicular, anterior and posterior cervical, axillary, suprascapular, supraspinal and ventral spinal (referred to as peri-aortic by some investigators) adipose tissues areas also labeled strongly with ^{18}F-FDG (Figure 2A).

β3 adrenergic receptor agonists can potently stimulate rodent and human BAT activity and, after a more extended exposure, can even lead to an increase in BAT volume (Cypess et al., 2015; Mirbolooki et al., 2014). Here we used daily injections of CL316,243 for 7 days to boost ^{18}F-FDG uptake by this more chronic β3 adrenergic stimulation in mice. Adipose tissue regions of high metabolic activity are apparent not only in the region containing the classical interscapular BAT and in the infrascapular areas, but also around supraclavicular, anterior and posterior cervical, axillary, suprascapular, supraspinal and ventral spinal regions (Figure 2B). Furthermore, strong ^{18}F-FDG positive regions are apparent in the anterior subcutaneous chest area compared to the PBS-treated control group. The 3D-images of the distribution of ^{18}F-FDG uptake in controls *vs.* β3 agonist-treated mice become anatomically better defined by overlaying the PET and corresponding CT images (Movies S2 and S3). Of note, there was no apparent ^{18}F-FDG uptake in the classical inguinal white adipose tissue (iWAT) region at baseline. Even after 7-days of β3 agonist treatment, it was hard to visualize this region by ^{18}F-FDG-PET/CT images (Figures 2A–B).

Cold exposure induces browning and beigeing of human adipose tissue and enhances consumption of glucose and fatty acids (Cypess et al., 2015; Townsend and Tseng, 2014). This reflects the ability of thermogenic adipose tissues to not only utilize glucose, but also to

avidly consume fatty acids. To differentially visualize the metabolically highly active fat pads in rodents, we also conducted SPECT/CT scanning in mice after the injection of the fatty acid tracer ^{123}I-BMIPP (Figures 2C–D). Mice housed at room temperature showed the strongest radiotracer accumulation in regions corresponding to the classical interscapular BAT, with additional signals around the anterior cervical, axillary, supraspinal and infrascapular regions. Furthermore, ^{123}I-BMIPP uptake was also apparent in the supraclavicular, suprascapular and ventral spinal areas. Even the classical inguinal WAT (iWAT) regions and the anterior subcutaneous region of the chest, displayed some tracer accumulation under basal conditions (Figure 2C). Moreover, β3 adrenergic stimulation enhanced fatty acid uptake in these fat pads, especially in the classical inguinal WAT, as well as in the anterior subcutaneous and suprascapular pads. This highlights that these three regions are prone to increased fatty acid consumption relative to other fat pads (Figure 2D). The SPECT/CT 3D display of the regions with high ^{123}I-BMIPP fatty acid uptake in control *vs.* β3 agonist treated mice provided a high level of precision as to where these fats pads are anatomically positioned (Movies S4 and S5).

[^{18}F]-fluoro-6-thia-heptadecanoic acid (^{18}F-FTHA) is another long-chain fatty acid substrate for fatty acid metabolism. We also tested imaging with ^{18}F-FTHA, but in our hands the images showed high background after uptake and relatively low resolution compared to ^{123}I-BMIPP -SPECT images (Figure S1). Therefore, considering both the better scanner resolution and improved targeting to the triglyceride pool, we reasoned that ^{123}I-BMIPP is a better tracer for our purposes.

Inducible Ablation of Adipocytes Prior to Labeled Glucose and Fatty Acid Imaging Tracer Uptake Delineates Metabolically Active Regions as Adipose Tissues

To distinguish adipose tissues from other metabolically active non-adipose tissue regions, we employed an inducible fat ablation model that we had previously described, the FAT-ATTAC model. The FAT-ATTAC model allows ablation of both white and brown adipocytes at any stage of development and in the adult mouse (Pajvani et al., 2005). As shown in Figure 3, control mice showed the expected patterns of ^{18}F-FDG glucose and ^{125}I-BMIPP fatty acid uptake as previously observed in Figures 2A and 2C (Figures 3A–B left-panels). In contrast, the lipodystrophic FAT-ATTAC mice displayed markedly reduced activity not only around the regions of the classical interscapular BAT, but also reduced signal in the infrascapular, supraclavicular, anterior and posterior cervical, axillary, suprascapular, supraspinal, anterior subcutaneous and ventral spinal adipose tissues areas (Figure 3A–B right-panels). Interestingly, the lipodystrophic mice instead increased the glucose and fatty acid uptake in brain, liver and muscle (Movies S6–S9). Based on the topographical information obtained from these models, we generated a representative composite image reflecting the locations of the main fat pads visualized by PET/CT and SPECT/CT, with blue arrows pointing towards the distinctly identifiable patches of metabolically active adipose tissues and yellow arrows indicating fat pads that display background signal levels of ^{18}F-FDG-PET/CT and ^{123}I-BMIPP-SPECT/CT (Figure 3C). These fat pads include classical iBAT, supraclavicular, anterior cervical, axillary, anterior subcutaneous, suprascapular, infrascapular, supraspinal, ventral spinal adipose tissues as well as inguinal WAT (iWAT).

Even though the classical epididymal WAT (eWAT) is well defined anatomically, they did not display any ^{18}F-FDG-PET/CT or ^{123}I-BMIPP-SPECT/CT based signals.

Histological Analysis Confirms Metabolically Active Regions as Adipose Tissues

To directly verify the nature of the tissues revealing strong signals by PET/CT and SPECT/CT, these tissues were isolated based on the position of the signal within the 3D-images obtained from PET/CT and SPECT/CT scans. In a first phase, we focused on the conventional fat pads, some of which displayed potent glucose and lipid uptake activity (Figure 4A). Hematoxylin-eosin (H&E) staining of regions isolated from these “classical” fat pads that include interscapular BAT (iBAT), inguinal WAT (iWAT) and epididymal WAT (eWAT) were performed. As shown in Figure 4B, control mice maintained at ambient temperature contained multilocular cells in the interscapular BAT region and unilocular/larger lipid morphology in the inguinal and epididymal WAT. Multilocular beige cells were detectable in the inguinal WAT region after β3 adrenergic stimulation or cold exposure. Even the eWAT region showed some low level of a “beige-like” phenotype after 7-days of β3 agonist treatment, even though not nearly as pronounced. These results confirm that the PET/CT and SPECT/CT image-guided isolation of adipose tissue has the potential to identify either brown or beige adipose tissues, while eWAT with its classical white adipose tissue phenotype does give rise to an easily detectable PET or SPECT signal.

We subsequently extended the histological analysis to the additional fat pads, including the supraclavicular, anterior cervical, axillary, anterior subcutaneous, suprascapular, infrascapular, supraspinal and ventral spinal adipose tissues as shown in the left panels of Figure 5. Each adipose depot is labeled to indicate its location in the cartoon with both frontal and lateral views. The histology as judged by H&E staining in control mice revealed multilocular cells in the supraclavicular, anterior cervical, axillary, infrascapular, supraspinal and ventral spinal adipose regions, while anterior subcutaneous and suprascapular areas displayed unilocular morphology (Figure 5 Second-left panel). Both β3 adrenergic and cold stimulation increased the frequency and extent of the multilocular cells in the BAT-like adipose tissues and triggered beigeing in the anterior subcutaneous and suprascapular areas. Immunoflorescent stains for UCP1 and PERILIPIN also indicated the morphology and nature of fat cells explored by PET and SCPECT imaging (Figure S2). These images suggest that the supraclavicular, anterior cervical, axillary, infrascapular, supraspinal and ventral spinal adipose tissues are likely to correspond to brown fat tissues, while the anterior subcutaneous and suprascapular adiposes appear to be “beige-like” tissues.

Expression Levels of WAT, BAT and Beige Marker Genes in image-guided fat pads

To further characterize these adipose tissues and classify them into white, brown or beige fat depots, a series of marker genes for these three types of adipose tissues were analyzed by qPCR (de Jong et al., 2015; Shao et al., 2016; Sharp et al., 2012; Walden et al., 2012; Wu et al., 2012). The classical iBAT, iWAT and eWAT pads from mice at baseline and after β3 adrenergic or cold stimulation were analyzed first as positive controls. As shown in Figure 6A, *Tcf21* is expressed only in eWAT, but not iBAT and iWAT. *Tcf21* expression levels in other fat tissues were very low, even after β3 adrenergic and cold stimulation. *Zic1,* recognized as a marker for BAT, showed expression in iBAT, but not in eWAT and iWAT.

Cold exposure, however, did not significantly change *Zic1* mRNA abundance in iBAT, while β3 adrenergic stimulation reduced it to some extent. *Zic1* expression is detected in supraclavicular, anterior cervical, axillary, infrascapular, supraspinal and ventral spinal adipose, while anterior subcutaneous and suprascapular adiposes displayed very low level of expression (Figure 6B). *Ucp1* was as expected highly abundant in iBAT at room temperature and did not significantly change upon β3 adrenergic stimulation or cold acclimation. In iWAT, *Ucp1* mRNA levels increased 66-fold and 206-fold after β3 agonist and 6°C treatment, with final levels reached comparable to those in iBAT. *Ucp1* expression was also increased in eWAT, but remained at much lower levels than in iBAT and iWAT (Figure 6C). Among the other fat pads, *Ucp1* was expressed to a lesser extent in anterior subcutaneous and suprascapular adipose depots, expressed at an intermediate level in supraclavicular, anterior cervical and axillary regions, and most highly expressed in the infrascapular, supraspinal and ventral spinal adipose in control mice at room temperature. Upon β3 adrenergic stimulation or 6°C treatment, expression levels of *Ucp1* increased in all of these fat depots. The increase is markedly more pronounced by cold compared to β3 agonist treatment. Interestingly, the *Ucp1* mRNA in the supraclavicular, anterior cervical, axillary, infrascapular, supraspinal and ventral spinal adipose tissues of cold stimulated mice reached similar levels as seen in iBAT. The increase of *Ucp1* in anterior subcutaneous and suprascapular adipose tissues is however lower, resembling more closely the situation in iWAT (Figure 6C). *Lhx8* was absent in eWAT, but its expression patterns in iBAT and iWAT were comparable. It showed trends towards a reduction in the presence of β3 adrenergic stimulation and no marked changes after cold acclimation. *Lhx8* was expressed throughout all other adipose tissues, and the expression patterns were similar to iBAT and iWAT (Figure 6D). *Tmem26*, *Cd137*, *Tbx1* and *Epsti1* are recognized gene markers of beige tissues (de Jong et al., 2015). As shown in Figure 6E–H, these 4 genes were expressed at markedly higher levels in iWAT than in iBAT and eWAT, where they were essentially absent. Anterior subcutaneous and suprascapular adipose depots displayed high expression under control conditions and showed a similar expression pattern as iWAT among all the fat pads. The expression levels of *Tmem26*, *Cd137*, *Tbx1* and *Epsti1* in supraclavicular, anterior cervical, axillary, infrascapular, supraspinal and ventral spinal adipose tissues were lower than in iWAT. Overall, the gene expression patterns of *Tcf21*, *Zic1, Ucp1, Lhx8, Tmem26*, *Cd137*, *Tbx1* and *Epsti1* indicate that the supraclavicular, anterior cervical, axillary, infrascapular, supraspinal and ventral spinal adipose tissues are “BAT-like” adipose tissues. In contrast, anterior subcutaneous and suprascapular adipose depots are more closely related to “beige-like” adipose tissues as judged by their gene expression patterns.

DISCUSSION

Our studies utilized ^{18}F-FDG and $^{123/125}$I-BMIPP as glucose and fatty acid analogue imaging tracers to map metabolically active adipose tissue regions in the mouse. With the help of CT-guided topological information, these areas include classical iBAT, classical iWAT, supraclavicular, anterior cervical, axillary, anterior subcutaneous, suprascapular, supraspinal, ventral spinal, infrascapular and peri-renal regions at baseline. ^{123}I-BMIPP-SPECT/CT additionally visualized classical subcutaneous WAT (iWAT) and anterior subcutaneous WAT, pads not readily visualized by ^{18}F-FDG-PET/CT imaging. In contrast,

no significant tracer accumulation was detected in the posterior cervical region by ^{123}I-BMIPP-SPECT/CT, but it was detectable in ^{18}F-FDG-PET/CT. Note that we chose terminology for anatomical locations of the fat pads mainly based on human anatomy as opposed to the more conventional terminology used in mice based on their neural axis. We used an inducible adipose tissue ablation model to confirm that these areas correspond to fat depots. Moreover, histological analysis as well as identification by marker genes analysis validate supraclavicular, anterior cervical, axillary, supraspinal, ventral spinal, infrascapular, peri-renal regions as BAT, and the anterior subcutaneous and suprascapular fat tissues as beige adipose tissue (Figure 7).

Imaging with ^{18}F-FDG-PET/CT and ^{123}I-BMIPP-SPECT/CT not only guided the anatomic dissection of the fat tissues, but also offers a functional assessment with respect to the avidity with which a given fad pad takes up carbohydrates and lipids. It seems that “beige-like” fat tissues are prone to show retention of fatty acids tracers more preferentially when compared to BAT (Figure 2). Focusing on the cervical fat pad regions, the analysis of morphology as well as marker gene expression does not reveal many differences between the two distinct regions of cervical fat (Figures S3 and S4). For this cervical area, ^{123}I-BMIPP fatty acid-based images show strong signal in the anterior cervical regions, but not nearly as much in the posterior cervical regions where ^{18}F-FDG routinely displays a strong signal in humans and to a lesser degree in mice (Figures 1 and 2). All of these differential uptake measurements are reflective of different substrate preferences in these fat pads. We focus here mostly on imaging activity obtained by PET and SPECT imaging and describe regions with signals that are distinctly above background. Anatomical features of brown and beige adipocytes are conventionally studied by dissection followed by histology in both humans and rodents (Cinti, 2009; Tran and Kahn, 2010). Imaging approaches employing radioactive substrates added an additional functional parameter to the conventional histological analysis. The combination of both techniques leads to the appreciation that humans have in fact cold-inducible adipose tissues that avidly take up radioactive tracers.

Here, we utilized ^{18}F-FDG-PET/CT guided dissection of metabolically very active regions in rodents to describe novel adipose tissues in the suprascapular, supraspinal, infrascapular and ventral spinal regions. The intensity of the tracer accumulation obtained in the imaging procedure reflects a relatively high metabolic activity. In fact, some of these fat pads (including the supraspinal and infrascapular regions) showed comparable activity to the classical interscapular BAT (Figures 2 and 3). Additionally we found uptake variability amongst our mice just as we have seen in clinical practice. We have undertaken a quantitative analysis of the signal in the various depots. The mouse-to-mouse variability produced relatively large standard deviations in the uptake of the label, confounding statistical significance values. Furthermore, the quantitation in absolute terms in the 3-dimensional space offers many challenges. Overall, β3-adrenergic agonist- and cold-induced increases in signal can indeed be observed. However, we have used this technique primarily to help us identify novel fat pads that have gone unreported to date, not to detect quantitative difference in uptake of label. We opted to provide a more quantitative assessment of the nature of these fat pads at the gene expression level.

Thermogenic adipose tissues are considered potential therapeutic targets due to their high capacity to dissipate excess energy as heat when properly stimulated (Sanchez-Gurmaches et al., 2016). One of the current problems in the field is the unavailability of an appropriate rodent model to characterize the respective human fat pads functionally. Therefore, we mapped adipose tissues in mice. As expected, there remain notable anatomical differences between rodents and humans. Human cervical BATs are mainly located in the back of the neck, and may extend from the base of the skull to the scapula. Comparable active regions in mice are seen in the more anterior cervical area extending to the supraclavicular region (Figures 1 and 2). On the other hand, mice show a more prominent infrascapular signal compared to humans. We also found that activity around the thoracic spine in humans is frequently at the junction with the ribs (paravertebral). While the ventral spinal location is observed in mice and man, the extension into the lumbar region is more frequently seen in mice. Furthermore, in mice, to date we did not observe the mediastinal activity that is observed in humans. Both species show the peri-renal distribution with some minor variations in its distribution - humans often have an active fat pad at the top of the cone of fat above the kidney (suprarenal) that can extend around and down towards the mid-line or away from the mid-line along the lateral peri-renal fat, while mice mostly show it medial to the kidney nearer to the spine.

While FDG is the most frequently used molecular imaging probe to identify active fat pads, other substrates have been used, either in small case series or incidentally observed to localize to fat. For example, ^{99m}Tc-Sestamibi, used clinically in cardiac perfusion imaging and parathyroid imaging, localizes in part according to mitochondrial density. It has been reported to localize in supraclavicular fat (Goetze et al., 2008). [^{123}I]-meta-iodobenzylguanidine (^{123}I-MIBG), a catecholamine analogue and a marker of sympathetic innervation, has been used in tandem with FDG to simultaneously visualize metabolic activity and innervation (Admiraal et al., 2013). [^{18}F]-fluoro-6-thia-heptadecanoic acid (^{18}F-FTHA) is a long chain fatty acid analogue PET imaging tracer that has been shown to localize to active fat pads (Ouellet et al., 2012). As discussed above, this tracer provided much less resolution. To our knowledge, this is the first study systematically studying fat uptake using ^{123}I-BMIPP. ^{123}I-BMIPP is clinically used to image cardiac metabolism (Giedd and Bergmann, 2011). It is transported into cells both passively based on lipid solubility and a CD36 mediated transport mechanism, trapped in the intracellular triglyceride pool after conversion to BMIPP-CoA, and to lesser extent, undergoes alpha-oxidation (Knapp and Kropp, 1999). This trapping mechanism makes it ideal for imaging. To our knowledge, this is the first study using $^{123/125}$I-BMIPP to systematically identify active fat pads to guide the dissection and further characterization of these fat pads. While both ^{123}I-BMIPP and ^{18}F-FTHA are fatty acid analogues, in contrast to ^{123}I-BMIPP, ^{18}F-FTHA uptake is mediated by the fatty acid transporter and then it is largely transported into the mitochondria by carnitine palmitoyl transferase and β-oxidation is initiated (DeGrado et al., 1991) but apparently incomplete (Knapp and Kropp, 1999). Its uptake is high in liver and heart, and its affinity for intracellular triglyceride pools is limited (Ci et al., 2006; Guiducci et al., 2007).

Our study with ^{123}I-BMIPP fatty acids shows preferentially uptake by thermogenic adipocytes that are prone to absorb fatty acids as a fuel. To our surprise, ^{123}I-BMIPP fatty

acid uptake was also observed in the classical iWAT locations at baseline and displayed even stronger uptake activity after β3 adrenergic stimulation (Figures 2C–D and Movies S4–S5). On the other hand, the uptake was hardly visible in iWAT on ^{18}F-FDG-PET/CT images, even after stimulation (Figures 2A–B and Movies S2–S3). This reflects the fact that classical iWAT may prefer fatty acids over glucose, different from the classical BAT. Similarly, the anterior subcutaneous, supraspinal, and ventral spinal (lower intra-abdominal part) regions identified as beige- and BAT-like, were more obvious on ^{123}I-BMIPP images than on ^{18}F-FDG on images (Figure 2 and Figures S2, S3). Peri-renal activity was also more frequently clearer on the ^{123}I-BMIPP scan. It is clear from systematically comparing glucose and fatty acid uptake in the different fat pads that each of these tissues has discrete substrate preference for one versus the other. However, future metabolic studies should more systematically evaluate substrate utilization and preference as our purpose here was to establish an atlas rather than metabolic flux. One additional caveat of focusing on differential uptake alone is that some of the fatty acids used by BAT and beige fat are thought to stem from hydrolysis of local triglyceride stores, which we do not address by our approach. An increased level of uptake of fatty acids by some depots may therefore reflect less local lipolysis. While substrate preference may be difficult to unambiguously assign, the differential signal intensities definitely reflect distinct cellular physiology in the different fat pads examined.

Furthermore, we have focused here exclusively on the fat distribution in male mice. Future studies will have to examine sexually dimorphic distributions in male vs. female mice, and will also have to examine the uptake of substrates under different metabolic conditions, such as feeding/fasting and obese versus lean.

Old estimates suggest that 50 g of maximally stimulated brown adipose tissue could account for up to 20% of daily energy expenditure in an adult human (Rothwell and Stock, 1983). Therefore, a better understanding of the location, quantity and activity of thermogenic adipose tissues and how to boost their metabolic activity would be helpful from both an anti-obesity and anti-diabetic treatment perspective. The exploration of novel thermogenic adipocytes in mice provides us a better understanding of fundamental map of active rodent BAT and beige tissues and how they may relate to their human counterparts. Various reports describe that external and internal regulators like cold, exercise, environmental cues, central nervous system, autonomic thermoregulatory pathways and neurotransmitters, transcriptional mediators, hormones and metabolites, eosinophils, alternatively activated macrophages and other cell types may control brown fat development and activation (browning) (Martinez de Morentin et al., 2014; Morrison and Madden, 2014; Qiu et al., 2014; Seale, 2015; Sidossis and Kajimura, 2015; Tupone et al., 2014). These players and interventions provide us with potential ways to increase thermogenesis and stave off metabolic disease.

In conclusion, the combination of avid ^{18}F-FDG glucose and ^{123}I-BMIPP fatty acid uptake with a morphological characterization and gene expression analysis for marker genes indicates that rodents show a surprising topological similarity to the distribution of brown and beige in humans.

STAR Methods

Contact for Reagent and Resource Sharing

Further information and requests for resources and reagents should be directed to and will be fulfilled by the Lead Contact, Philipp E. Scherer (Philipp.Scherer@UTSouthwestern.edu).

"Raw" (DICOM) compatible files of all images and movies that enable investigators to reconstruct the data into images have been uploaded to Mendeley and is accessible under doi:10.17632/9ykm4g4gp4.1.

Experimental Model and Subject Details

Animal Models

General animal study details: All animal procedures have been approved by the Institutional Animal Care and Use Committee of UT Southwestern Medical Center at Dallas. Male C57BL/6 mice were purchased from the Jackson Laboratory. All animals were bred and maintained under specific pathogen free conditions. Cages and water were autoclaved. Mice were kept on a 12 hr light-dark cycle in a temperature-controlled environment (room temperature: 22°C or cold exposure: 6°C). Mice had free to access water and w ere fed on a standard chow diet (number 5058, LabDiet). 9- to 15-week-old male C57BL/6 mice were used for indicated experiments. The investigators were not blinded to the animal information through the procedures. There were no exclusions of any data for the reported results. All imaging experiments were performed minimally in duplicate.

Inducible fat ablation (FAT-ATTAC) mice: Inducible fat ablation (FAT-ATTAC) mice (Pajvani et al., 2005) were generated in the genetic background of FVB mice and characterized in our laboratory. We administered AP21087 (Ariad Pharmaceuticals) as dimerizer or vehicle (4% ethanol, 10% PEG-400, 2% Tween-20 in water) every 3 d by intraperitoneal injection at a dose of 0.2 μg/g body weight for 2 weeks. Experiments were performed in 9- to 15-week-old male FAT-ATTAC mice.

Method Details

Human Subject PET/CT Imaging—Retrospective review was performed of whole body PET/CT scans obtained in routine clinical practice of one of the authors. The study was approved by the IRB at UT Southwestern Medical Center. An illustrative case was chosen for this report. Uptake rooms are maintained at 72°F. This patient was an 18y/o male with calculated BMI of 21.8 and no previous procedures. Selection of this case was made to show the broad spectrum of fat pads that can be seen by FDG PET.

β3 Agonist Treatment and Cold Stimulation—9- to 12-week-old male mice were treated with β3 agonist (CL-316243, Sigma) at 1 mg/kg body weight daily by intraperitoneal injections for 7 d while on a chow diet. For cold exposure experiments, 9- to 12-week-old male C57BL/6 mice were kept in cages individually and maintained on a chow diet. Mice were housed in a cold cabinet (6 °C) for 3 weeks with free access to food and water.

Radiotracers—[^{18}F]-fluorodeoxyglucose (^{18}F-FDG) was purchased from PETNET (Dallas, TX). The preparation of [$^{123/125}$I]-β-Methyl-*p*-iodophenyl-pentadecanoic acid ($^{123/125}$I-BMIPP) followed a previously published procedure (Goodman et al., 1984). Briefly, the BMPPA precursor (1.7 mg, 5 μmol) was activated by thallium trifluoroacetate (5.4 mg, 10 μmol) in TFA overnight, followed by reaction with radioactive iodine (^{123}I or ^{125}I, 10–20 mCi) plus potassium iodide (0.83 mg, 5 μmol). After ethyl ether extraction and C18 cartridge purification, the radiochemical identity and purity were assessed via radio thin layer chromatography (silica gel plate, hexane: ethyl ether: acetic acid=60:40:1, R_f = 0.5–0.6, >99%). The final product was formulated in warm 4% BSA saline solution for animal injection. The radiosynthesis of ^{18}F-FTHA was carried out in a GE TRACERLab automated synthesizer, following the previously reported procedure (Degrado, 1991). The precursor to ^{18}F-FTHA was purchased from ABX advanced biochemical compounds. The purified ^{18}F-FTHA was formulated in 4% BSA saline solution for animal use.

Mouse PET/CT and SPECT/CT Scanning for 3D-images—Mice PET-CT imaging studies were performed on a Siemens Inveon PET-CT Multimodality System (Hao et al., 2013). In brief, mice were fasted overnight and lightly anesthetized using 3% isofluorane at room temperature to facilitate radiotracer administration. After the intravenous injection of ~ 37 MBq (100 μCi) of ^{18}F-FDG was injected into the tail vein and the animal was permitted to roam freely in the cage during a 1 hour uptake time. Subsequently the animal was placed onto the imaging bed under 2% isofluorane anesthesia for the duration of imaging. After acquiring CT images at 80 kV and 500 μA with a focal spot of 58 μm, with a binning factor of 1:x, a whole body PET scan was acquired. Co-registration of the reconstructed CT and PET images and image analysis were done using the manufacturer's software. For PET quantification, the regions of interest (ROI) were selected using CT images as guides. The resulting quantitative data were expressed as %ID/g.

SPECT/CT imaging was performed using NanoSPECT/CT Plus System equipped with 4 detectors. All animals were fasted overnight prior to imaging. After the intravenous injection of ~ 175 MBq (~500 μCi) of ^{123}I-BMIPP or ^{125}I-BMIPP, SPECT images were acquired at 1 hour post injection. The SPECT data were collected with 4 detector arrays collimated with 9-pinhole aperture plates giving a post-reconstruction resolution of 0.400mm. Images were acquired for 70 seconds in a standard anterior projection in list mode, at a rate of 1 frame per second. The CT imaging was performed using 360 projections per rotation with 45kVp, 1000 ms exposure, and the binning factor of 1:4. After co-registration of the CT and SPECT images, a cylindrical region of interest (ROI) was drawn, encompassing the organs in all planes containing the organs. The total activity in the ROI was quantified as percentage injected dose per gram (%ID/g) by normalizing the signal imaged at a given location for the amount of tracer injected into the subject. There was a minimum of (n=3) mice per experimental group and radiotracer in the study. During the uptake period, the mice were conscious. After the 1 hour uptake period, they were anesthetized with isoflurane for imaging.

Histology and Immunofluorescence—Fat pads were excised and fixed in 10% PBS-buffered formalin for 24 h. After paraffin embedding and sectioning (5 μm), tissues were

stained with H&E. For immunohistochemistry, paraffin-embedded sections were stained using antibodies to UCP1 (ab10983, Abcam, 1:200) and PERILIPIN (20R-PP004, Fitzgerald, 1:1000); the secondary antibodies used were goat anti-rabbit Alexa Fluor 488 (A-11008, Invitrogen, 1:500) and goat anti-guinea pig Alexa Fluor 647 1:500 (A-21450, Invitrogen, 1:500) (Vishvanath et al., 2016). Briefly, sections were thawed for 5 minutes in PBS containing 0.1% Triton X-100 (PBS-T), and then blocked/permeabilized for 30 minutes in PBS containing 10% normal goat serum and 0.5% Triton X-100. Primary antibodies were then diluted in PBS containing 10% normal goat serum and 0.1% Triton X-100 and added to sections overnight at 4°C. Following washing in PBS-T, slides were then incubated with secondary antibodies diluted in PBS containing 10% normal goat serum and 0.1% Triton X-100 for 1 hour at 37°C . Washed slides were then mounted with Prolong Anti-Fade mounting medium containing DAPI (Invitrogen).

Quantitative Real-time RT-PCR—Tissues were excised from mice and snap frozen. Total RNA was isolated after tissue homogenization in TRIzol (Invitrogen) and then isolated using an RNeasy RNA extraction kit (Qiagen). Complementary DNA was prepared by reverse transcribing 1 μg of RNA with iScrip cDNA Synthesis Kit (BioRad). Supplemental Table 1 lists the primer sets used for quantitative RT-PCR. Results were calculated using the threshold cycle method with *TFIIB* used for normalization.

Quantification and Statistical Analysis

The comparisons among three groups were carried out using one way ANOVA and appropriate post hoc tests using GraphPad Prism. Data presented were normally distributed, the data variance among comparable experimental groups was similar. All data were presented as mean ± SD, and p values < 0.05 was considered statistically significant. The calculated statistical parameters can be found in the figure legends. The number of mice used per experiment is stated in each figure legend.

Supplementary Material

Refer to Web version on PubMed Central for supplementary material.

Acknowledgments

This study was supported by NIH Grants R01-DK086629, R01-DK55758 and P01-DK088761, R01-DK092163, and discretionary funds from the department of Radiology. Dr. Fang Zhang is supported by the Visiting Scholar Program of the Chinese Academy of Sciences. The purchase of the NanoSPECT-CT scanner was supported by NIH shared instrumentation grant number 1S10RR029674-01. The authors acknowledge the generous support of a private donor that allowed the purchase of the Inveon PET-CT system. The authors express gratitude to Pam Curry in Creative Services in the department of Radiology and Taha Azimaie for assistance in preparing figures.

References

Admiraal WM, Holleman F, Bahler L, Soeters MR, Hoekstra JB, Verberne HJ. Combining 123I-metaiodobenzylguanidine SPECT/CT and 18F-FDG PET/CT for the assessment of brown adipose tissue activity in humans during cold exposure. J Nucl Med. 2013; 54:208–212. [PubMed: 23318291]

Betz MJ, Enerback S. Human Brown Adipose Tissue: What We Have Learned So Far. Diabetes. 2015; 64:2352–2360. [PubMed: 26050667]

Cannon B, Nedergaard J. Brown adipose tissue: function and physiological significance. Physiol Rev. 2004; 84:277–359. [PubMed: 14715917]

Ci X, Frisch F, Lavoie F, Germain P, Lecomte R, van Lier JE, Benard F, Carpentier AC. The effect of insulin on the intracellular distribution of 14(R,S)-[18F]Fluoro-6-thia-heptadecanoic acid in rats. Mol Imaging Biol. 2006; 8:237–244. [PubMed: 16791750]

Cinti S. Transdifferentiation properties of adipocytes in the adipose organ. Am J Physiol Endocrinol Metab. 2009; 297:E977–986. [PubMed: 19458063]

Cohen P, Spiegelman BM. Cell biology of fat storage. Mol Biol Cell. 2016; 27:2523–2527. [PubMed: 27528697]

Cypess AM, Lehman S, Williams G, Tal I, Rodman D, Goldfine AB, Kuo FC, Palmer EL, Tseng YH, Doria A, et al. Identification and importance of brown adipose tissue in adult humans. N Engl J Med. 2009; 360:1509–1517. [PubMed: 19357406]

Cypess AM, Weiner LS, Roberts-Toler C, Franquet Elia E, Kessler SH, Kahn PA, English J, Chatman K, Trauger SA, Doria A, Kolodny GM. Activation of human brown adipose tissue by a beta3-adrenergic receptor agonist. Cell Metab. 2015; 21:33–38. [PubMed: 25565203]

de Jong JM, Larsson O, Cannon B, Nedergaard J. A stringent validation of mouse adipose tissue identity markers. Am J Physiol Endocrinol Metab. 2015; 308:E1085–1105. [PubMed: 25898951]

Degrado TR. Synthesis of 14 (R,S)-[18F]fluoro-6-thia-heptadecanoic acid (FTHA). J Label Compd Radiopharm. 1991; 29:989–995.

DeGrado TR, Coenen HH, Stocklin G. 14(R,S)-[18F]fluoro-6-thia-heptadecanoic acid (FTHA): evaluation in mouse of a new probe of myocardial utilization of long chain fatty acids. J Nucl Med. 1991; 32:1888–1896. [PubMed: 1919727]

Enerback S. Human brown adipose tissue. Cell Metab. 2010; 11:248–252. [PubMed: 20374955]

Giedd KN, Bergmann SR. Fatty acid imaging of the heart. Curr Cardiol Rep. 2011; 13:121–131. [PubMed: 21240641]

Goetze S, Lavely WC, Ziessman HA, Wahl RL. Visualization of brown adipose tissue with 99mTc-methoxyisobutylisonitrile on SPECT/CT. J Nucl Med. 2008; 49:752–756. [PubMed: 18413387]

Goodman MM, Kirsch G, Knapp FF Jr. Synthesis and evaluation of radioiodinated terminal p-iodophenyl-substituted alpha- and beta-methyl-branched fatty acids. J Med Chem. 1984; 27:390–397. [PubMed: 6699884]

Guiducci L, Gronroos T, Jarvisalo MJ, Kiss J, Viljanen A, Naum AG, Viljanen T, Savunen T, Knuuti J, Ferrannini E, et al. Biodistribution of the fatty acid analogue 18F-FTHA: plasma and tissue partitioning between lipid pools during fasting and hyperinsulinemia. J Nucl Med. 2007; 48:455–462. [PubMed: 17332624]

Hany TF, Gharehpapagh E, Kamel EM, Buck A, Himms-Hagen J, von Schulthess GK. Brown adipose tissue: a factor to consider in symmetrical tracer uptake in the neck and upper chest region. Eur J Nucl Med Mol Imaging. 2002; 29:1393–1398. [PubMed: 12271425]

Hao G, Du Y, Zhou XJ, Guo J, Sun X, Mohan C, Oz OK. Serial non-invasive assessment of antibody induced nephritis in mice using positron emission tomography. PLoS One. 2013; 8:e57418. [PubMed: 23460853]

Harms M, Seale P. Brown and beige fat: development, function and therapeutic potential. Nat Med. 2013; 19:1252–1263. [PubMed: 24100998]

Jensen MD. Adipose tissue and fatty acid metabolism in humans. J R Soc Med. 2002; 95(Suppl 42):3–7.

Knapp FF Jr, Kropp J. BMIPP-design and development. Int J Card Imaging. 1999; 15:1–9. [PubMed: 10453397]

Martinez de Morentin PB, Gonzalez-Garcia I, Martins L, Lage R, Fernandez-Mallo D, Martinez-Sanchez N, Ruiz-Pino F, Liu J, Morgan DA, Pinilla L, et al. Estradiol regulates brown adipose tissue thermogenesis via hypothalamic AMPK. Cell Metab. 2014; 20:41–53. [PubMed: 24856932]

Mirbolooki MR, Constantinescu CC, Pan ML, Mukherjee J. Quantitative assessment of brown adipose tissue metabolic activity and volume using 18F-FDG PET/CT and β3-adrenergic receptor activation. EJNMMI Res. 2011; 1:30. [PubMed: 22214183]

Mirbolooki MR, Upadhyay SK, Constantinescu CC, Pan ML, Mukherjee J. Adrenergic pathway activation enhances brown adipose tissue metabolism: a [(1)(8)F]FDG PET/CT study in mice. Nucl Med Biol. 2014; 41:10–16. [PubMed: 24090673]

Morrison SF, Madden CJ. Central nervous system regulation of brown adipose tissue. Compr Physiol. 2014; 4:1677–1713. [PubMed: 25428857]

Nedergaard J, Bengtsson T, Cannon B. Unexpected evidence for active brown adipose tissue in adult humans. Am J Physiol Endocrinol Metab. 2007; 293:E444–452. [PubMed: 17473055]

Orava J, Nuutila P, Lidell ME, Oikonen V, Noponen T, Viljanen T, Scheinin M, Taittonen M, Niemi T, Enerback S, Virtanen KA. Different metabolic responses of human brown adipose tissue to activation by cold and insulin. Cell Metab. 2011; 14:272–279. [PubMed: 21803297]

Ouellet V, Labbe SM, Blondin DP, Phoenix S, Guerin B, Haman F, Turcotte EE, Richard D, Carpentier AC. Brown adipose tissue oxidative metabolism contributes to energy expenditure during acute cold exposure in humans. J Clin Invest. 2012; 122:545–552. [PubMed: 22269323]

Pajvani UB, Trujillo ME, Combs TP, Iyengar P, Jelicks L, Roth KA, Kitsis RN, Scherer PE. Fat apoptosis through targeted activation of caspase 8: a new mouse model of inducible and reversible lipoatrophy. Nat Med. 2005; 11:797–803. [PubMed: 15965483]

Peterson LR, Gropler RJ. Radionuclide imaging of myocardial metabolism. Circ Cardiovasc Imaging. 2010; 3:211–222. [PubMed: 20233863]

Qiu Y, Nguyen KD, Odegaard JI, Cui X, Tian X, Locksley RM, Palmiter RD, Chawla A. Eosinophils and type 2 cytokine signaling in macrophages orchestrate development of functional beige fat. Cell. 2014; 157:1292–1308. [PubMed: 24906148]

Rosen ED, Spiegelman BM. Adipocytes as regulators of energy balance and glucose homeostasis. Nature. 2006; 444:847–853. [PubMed: 17167472]

Rothwell NJ, Stock MJ. Luxuskonsumption, diet-induced thermogenesis and brown fat: the case in favour. Clin Sci (Lond). 1983; 64:19–23. [PubMed: 6337007]

Saito M, Okamatsu-Ogura Y, Matsushita M, Watanabe K, Yoneshiro T, Nio-Kobayashi J, Iwanaga T, Miyagawa M, Kameya T, Nakada K, et al. High incidence of metabolically active brown adipose tissue in healthy adult humans: effects of cold exposure and adiposity. Diabetes. 2009; 58:1526–1531. [PubMed: 19401428]

Sanchez-Gurmaches J, Hung CM, Guertin DA. Emerging Complexities in Adipocyte Origins and Identity. Trends Cell Biol. 2016; 26:313–326. [PubMed: 26874575]

Scherer PE. Adipose tissue: from lipid storage compartment to endocrine organ. Diabetes. 2006; 55:1537–1545. [PubMed: 16731815]

Scherer PE. The Multifaceted Roles of Adipose Tissue-Therapeutic Targets for Diabetes and Beyond: The 2015 Banting Lecture. Diabetes. 2016; 65:1452–1461. [PubMed: 27222389]

Seale P. Transcriptional Regulatory Circuits Controlling Brown Fat Development and Activation. Diabetes. 2015; 64:2369–2375. [PubMed: 26050669]

Shao M, Ishibashi J, Kusminski CM, Wang QA, Hepler C, Vishvanath L, MacPherson KA, Spurgin SB, Sun K, Holland WL, et al. Zfp423 Maintains White Adipocyte Identity through Suppression of the Beige Cell Thermogenic Gene Program. Cell Metab. 2016; 23:1167–1184. [PubMed: 27238639]

Sharp LZ, Shinoda K, Ohno H, Scheel DW, Tomoda E, Ruiz L, Hu H, Wang L, Pavlova Z, Gilsanz V, Kajimura S. Human BAT possesses molecular signatures that resemble beige/brite cells. PLoS One. 2012; 7:e49452. [PubMed: 23166672]

Sidossis L, Kajimura S. Brown and beige fat in humans: thermogenic adipocytes that control energy and glucose homeostasis. J Clin Invest. 2015; 125:478–486. [PubMed: 25642708]

Taki J, Matsunari I. Metabolic imaging using SPECT. Eur J Nucl Med Mol Imaging. 2007; 34(Suppl 1):S34–48. [PubMed: 17479263]

Townsend KL, Tseng YH. Brown fat fuel utilization and thermogenesis. Trends Endocrinol Metab. 2014; 25:168–177. [PubMed: 24389130]

Tran TT, Kahn CR. Transplantation of adipose tissue and stem cells: role in metabolism and disease. Nat Rev Endocrinol. 2010; 6:195–213. [PubMed: 20195269]

Tupone D, Madden CJ, Morrison SF. Autonomic regulation of brown adipose tissue thermogenesis in health and disease: potential clinical applications for altering BAT thermogenesis. Front Neurosci. 2014; 8:14. [PubMed: 24570653]

van Marken Lichtenbelt WD, Vanhommerig JW, Smulders NM, Drossaerts JM, Kemerink GJ, Bouvy ND, Schrauwen P, Teule GJ. Cold-activated brown adipose tissue in healthy men. N Engl J Med. 2009; 360:1500–1508. [PubMed: 19357405]

Virtanen KA, Lidell ME, Orava J, Heglind M, Westergren R, Niemi T, Taittonen M, Laine J, Savisto NJ, Enerback S, Nuutila P. Functional brown adipose tissue in healthy adults. N Engl J Med. 2009; 360:1518–1525. [PubMed: 19357407]

Vishvanath L, MacPherson KA, Hepler C, Wang QA, Shao M, Spurgin SB, Wang MY, Kusminski CM, Morley TS, Gupta RK. Pdgfrbeta+ Mural Preadipocytes Contribute to Adipocyte Hyperplasia Induced by High-Fat-Diet Feeding and Prolonged Cold Exposure in Adult Mice. Cell Metab. 2016; 23:350–359. [PubMed: 26626462]

Walden TB, Hansen IR, Timmons JA, Cannon B, Nedergaard J. Recruited vs. nonrecruited molecular signatures of brown, "brite," and white adipose tissues. Am J Physiol Endocrinol Metab. 2012; 302:E19–31. [PubMed: 21828341]

Wang X, Minze LJ, Shi ZZ. Functional imaging of brown fat in mice with 18F-FDG micro-PET/CT. J Vis Exp. 2012

Wu J, Bostrom P, Sparks LM, Ye L, Choi JH, Giang AH, Khandekar M, Virtanen KA, Nuutila P, Schaart G, et al. Beige adipocytes are a distinct type of thermogenic fat cell in mouse and human. Cell. 2012; 150:366–376. [PubMed: 22796012]

Highlights

- Rodents and humans share topological similarity of thermogenic fat depots
- PET/CT and SPECT/CT differentially highlight newly identified fat pads in mice
- Histological and gene expression analysis confirm the regions as bona fide fat pads
- SPECT/CT with lipid tracers may reveal additional BAT and beige depots in humans

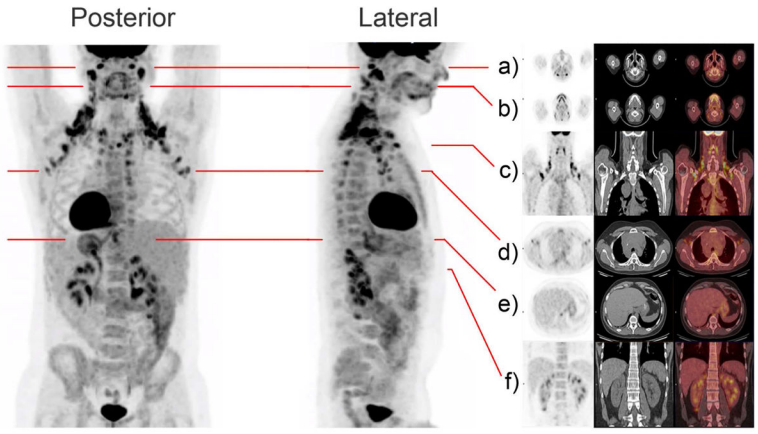

Figure 1. Regions of High Level Glucose Uptake in Humans as Assessed by ^{18}F-FDG-PET/CT

Metabolic activity in thermogenic tissues is demonstrated in this subject imaged with integrated [^{18}F]-Fluorodeoxyglucose-Positron Emission Tomography–Computed Tomography (^{18}F-FDG-PET/CT) at room temperature. Frontal and lateral maximal PET intensity projection images in an adult male subject show distribution of glucose uptake by its image tracer ^{18}F-FDG. In this subject, prominent FDG retention is shown in the cervical, supraclavicular, axillary, intercostal, mediastinal, ventral spinal, and peri-renal areas. Paravertebral tissue is also activated. Fat pads are also illustrated in multi-level transaxial or coronal PET/CT images (a–f) are shown in the Supplemental Movie (Movie S1).

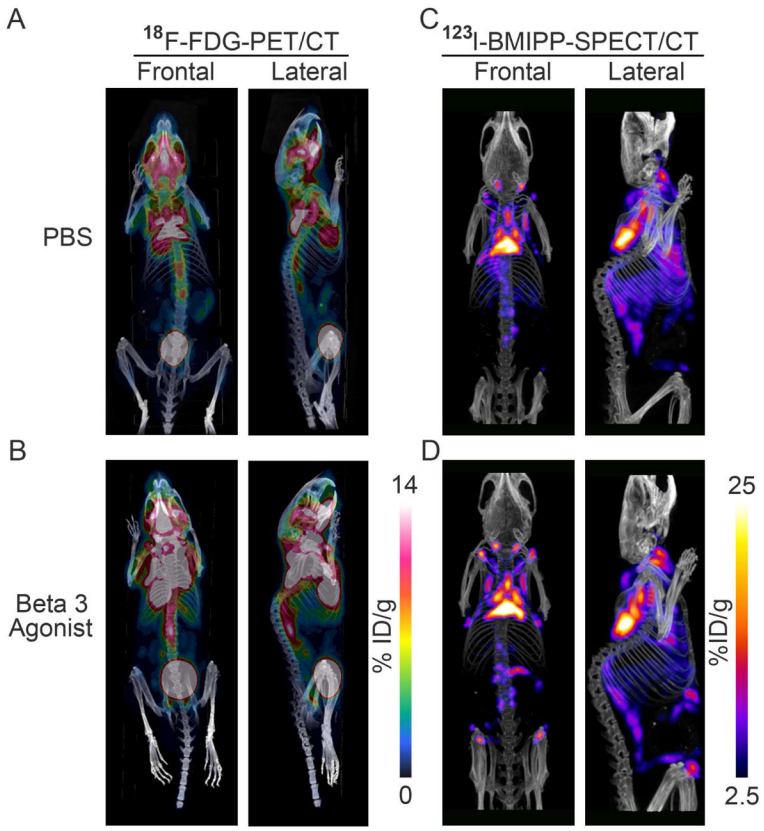

Figure 2. Anatomical Location of Metabolically Active Fat Pads as Assessed by 3D-images of PET/CT with ^{18}F-FDG for Glucose Uptake and SPECT/CT with ^{123}I-BMIPP for Fatty Acid Uptake

A-B. The left panels show the ^{18}F-FDG-PET/CT images of glucose uptake and distribution in the thermogenic tissues of an adult mouse kept at room temperature treated with 7-days PBS (upper-left panels, A) or β3 agonist (down-left panels, B). C–D. The right panels show the ^{123}I-BMIPP-SPECT/CT scanning for the patterns of fatty acid uptake in the metabolic active tissues of an adult mouse kept at room temperature after 7-days PBS treatment (upper-right panels, C) or β3 adrenergic stimulation. (lower-right panels, D). In each case, representative images for n=3 repeats are shown.

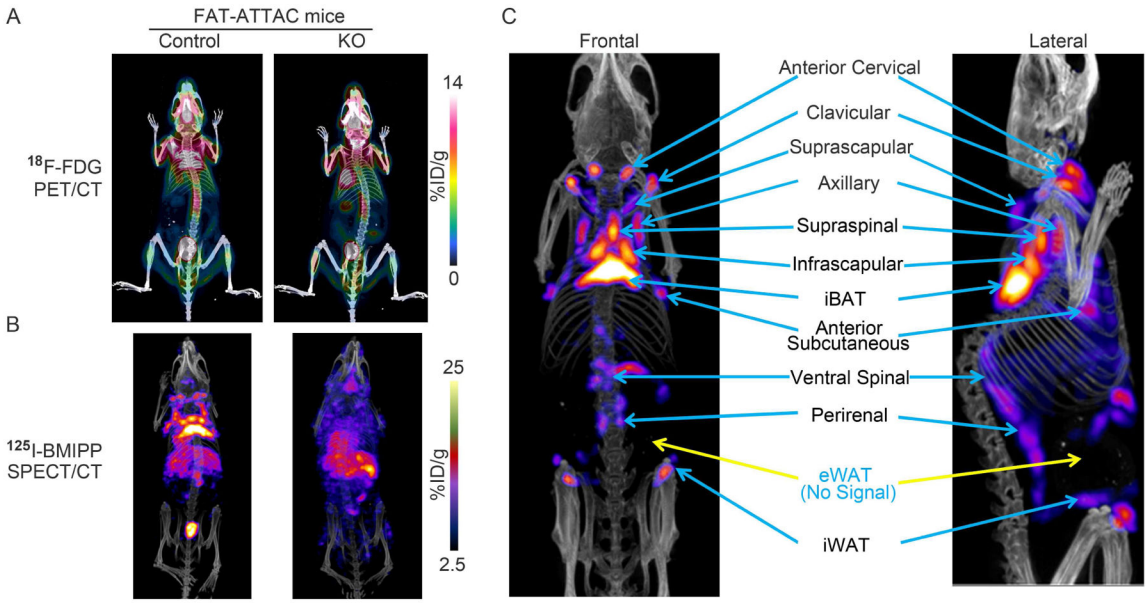

Figure 3. Signal intensity in a Lipodystrophic Rodent Model

A. A model of inducible lipodystrophy (the "FAT-ATTAC mouse") selectively loses adipocyte-derived signals upon ^{18}F-FDG injection compared to control. **B**. SPECT/CT imaging of the FAT-ATTAC lipodystrophic mouse confirms the identity of signals as adipocyte-derived ^{125}I-BMIPP uptake. **C**. The main metabolically active adipose tissues indicated with blue arrows in an adult mouse model stimulated by β3-adrenergic agonist for 7 days. Blue color label with yellow arrows indicate fat pads that display background signal levels of ^{18}F-FDG-PET/CT and ^{123}I-BMIPP-SPECT/CT. In each case, representative images for n=3 repeats are shown.

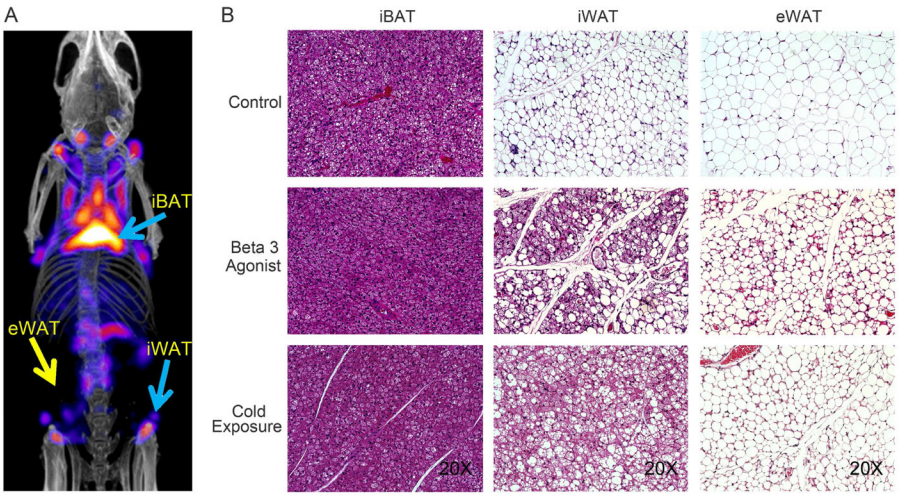

Figure 4. Histological Analysis of interscapular BAT, inguinal and epididymal fat tissues

A. Locations of interscapular BAT (iBAT), inguinal WAT (iWAT) and epididymal WAT (eWAT) depots indicated with blue arrows or yellow arrows display differential levels of fatty acid uptake after 7-days β3 adrenergic stimulation. **B**. Histological analysis of tissues highlights the expected phenotype of these “classic” adipose tissues from control, β3 agonist - treated and cold-stimulated mice. The presented images are representative for n=4 repeats of the histological analysis.

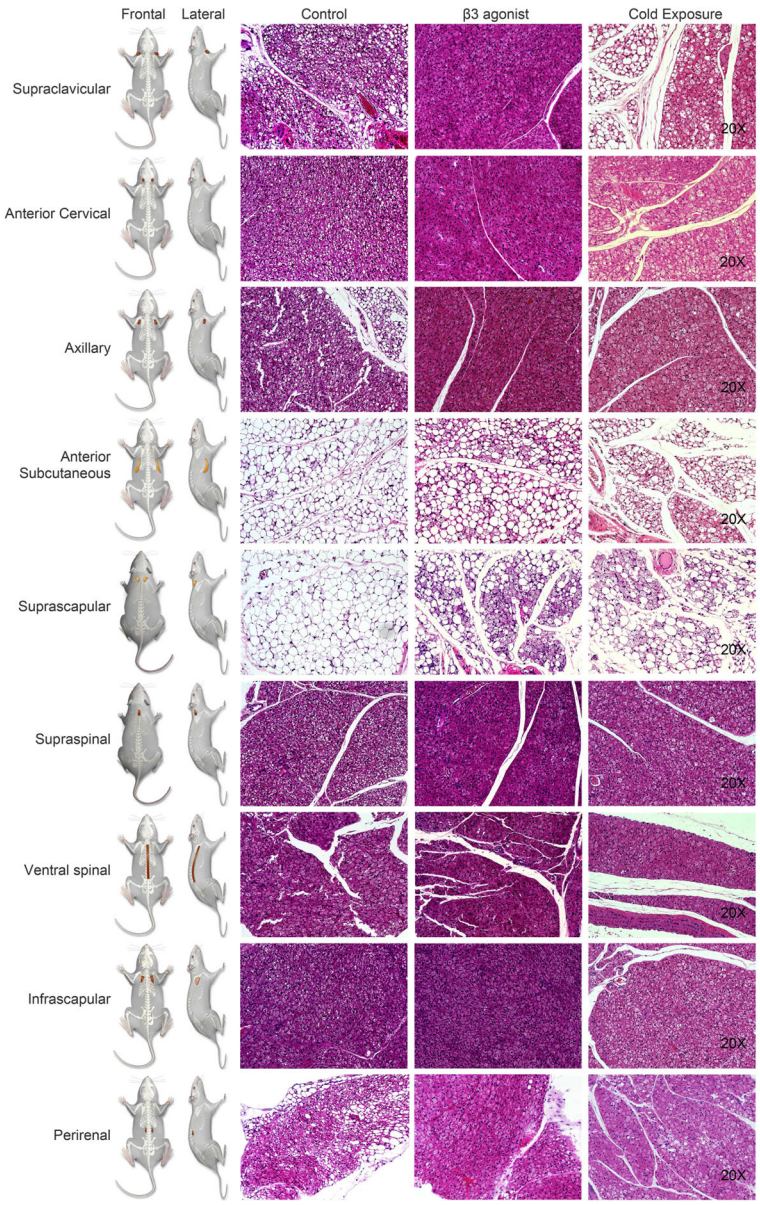

Figure 5. Histological Analysis of Additional Fat Pads at Baseline, β3 Agonist – Treated and Cold-Stimulated Mice

The images explore a series of additional regions of high metabolic activity around supraclavicular, anterior cervical, axillary, anterior subcutaneous, suprascapular, supraspinal, ventral spinal, infrascapular regions and in the peri-renal area as indicated in the cartoon. Clearly apparent are the unilocular resp. multilocular characteristics of each of the fat pads of control, β3 agonist-treated and cold-stimulated mice. The presented images are representative for n=4 repeats of the histological analysis

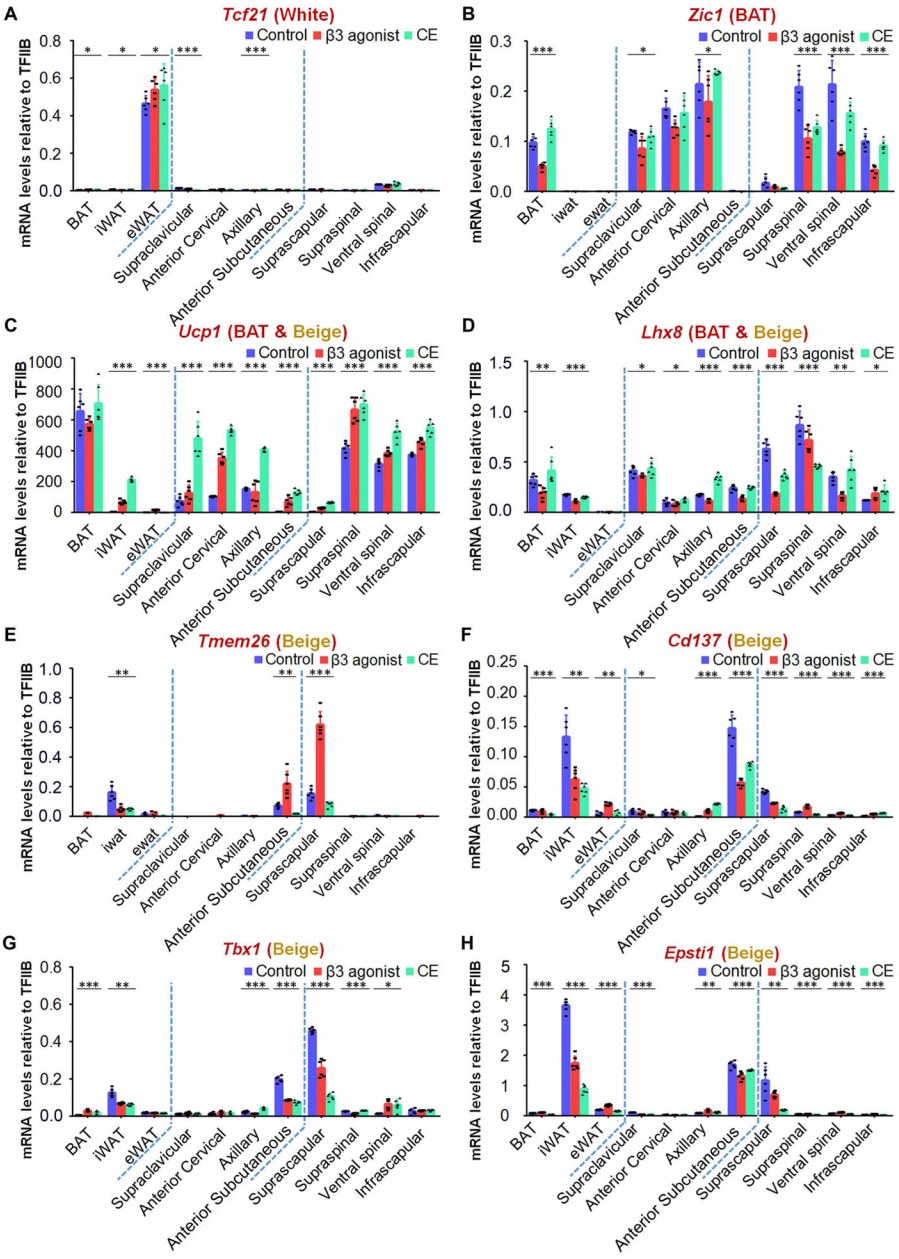

Figure 6. Expression Levels of Marker Genes Classify the Newly Isolated Fat Pads into the Three Categories of Fat Pads including WAT, BAT and Beige

A series of marker genes including *Tcf21* for WAT, *Zic1* for BAT depots, *Ucp1* and *Lhx8* for BAT and beige depots and *Tmem26*, *Cd137*, *Tbx1* and *Epsti1* for beige depots were used to examine the mRNA expression patterns of the newly identified fat pads, including supraclavicular, anterior cervical, axillary, anterior subcutaneous, suprascapular, supraspinal, ventral spinal, infrascapular regions and in the perirenal area in mice under control, β3 agonist-treated and cold-stimulated conditions (n=6). Results are shown as mean ± SD, *p <0.05, **p < 0.01 and ***p < 0.001.

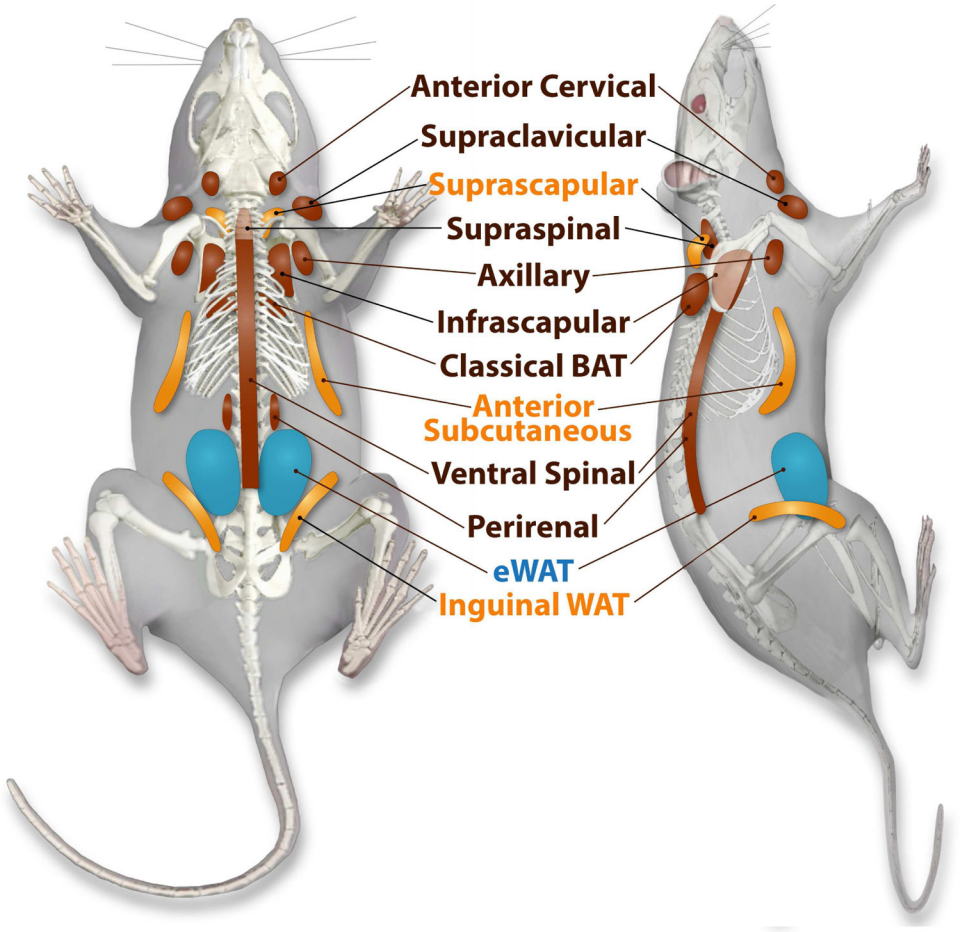

Figure 7. Location of Metabolically Identified and Histologically Confirmed Fat Pads

White adipose tissues indicated in blue, fat pads with the ability to beige are in yellow, and more classical brown adipose tissue-like fat pads are indicated in brown.